

Gemcitabine Mechanism of Action Confounds Early Assessment of Treatment Response by 3'-Deoxy-3'-[¹⁸F]Fluorothymidine in Preclinical Models of Lung Cancer

Sonja Schelhaas¹, Annelena Held¹, Lydia Wachsmuth², Sven Hermann¹, Davina J. Honess³, Kathrin Heinzmann³, Donna-Michelle Smith³, John R. Griffiths³, Cornelius Faber², and Andreas H. Jacobs^{1,4}

Abstract

3'-Deoxy-3'-[¹⁸F]fluorothymidine positron emission tomography ([¹⁸F]FLT-PET) and diffusion-weighted MRI (DW-MRI) are promising approaches to monitor tumor therapy response. Here, we employed these two imaging modalities to evaluate the response of lung carcinoma xenografts in mice after gemcitabine therapy. Caliper measurements revealed that H1975 xenografts responded to gemcitabine treatment, whereas A549 growth was not affected. In both tumor models, uptake of [¹⁸F]FLT was significantly reduced 6 hours after drug administration. On the basis of the gemcitabine concentration and [¹⁸F]FLT excretion measured, this was presumably related to a direct competition of gemcitabine with the radiotracer for cellular uptake. On day 1 after therapy, [¹⁸F]FLT uptake was increased in both models, which was correlated with thymidine kinase 1 (TK1) expression.

Two and 3 days after drug administration, [¹⁸F]FLT uptake as well as TK1 and Ki67 expression were unchanged. A reduction in [¹⁸F]FLT in the responsive H1975 xenografts could only be noted on day 5 of therapy. Changes in ADC_{mean} in A549 xenografts 1 or 2 days after gemcitabine did not seem to be of therapy-related biological relevance as they were not related to cell death (assessed by caspase-3 IHC and cellular density) or tumor therapy response. Taken together, in these models, early changes of [¹⁸F]FLT uptake in tumors reflected mechanisms, such as competing gemcitabine uptake or gemcitabine-induced thymidylate synthase inhibition, and only reflected growth-inhibitory effects at a later time point. Hence, the time point for [¹⁸F]FLT-PET imaging of tumor response to gemcitabine is of crucial importance. *Cancer Res*; 76(24); 7096–105. ©2016 AACR.

Introduction

In anticancer therapy, many efforts are made to detect response or resistance to treatment at an early time point. This enables an early shift of the therapy regimen, which allows for the reduction of side effects, an optimized therapy for the patient, and a reduction of costs for the health care system. Molecular imaging is a valuable tool to noninvasively and longitudinally follow biological and molecular processes within the body. In tumors,

these processes may shed light on therapy response. Consequently, use of appropriate imaging biomarkers might help to evaluate anticancer therapies in clinical trials. 3'-Deoxy-3'-[¹⁸F]fluorothymidine ([¹⁸F]FLT) is a radiotracer that is an analogue of thymidine, an essential building block of DNA. It is transported into cells in an analogous way to thymidine and is then phosphorylated by thymidine kinase 1 (TK1). The phosphorylated form of [¹⁸F]FLT is not incorporated into DNA and the tracer is retained within the cell. Hence, [¹⁸F]FLT accumulation is a readout of thymidine salvage pathway activity (1). PET with [¹⁸F]FLT is frequently correlated with cellular markers of proliferation (2) and thus can elucidate the proliferative status of rapidly growing tissue. [¹⁸F]FLT-PET is beginning to be recognized in the clinic for monitoring response to anticancer agents (3), as reductions in proliferation occur prior to reductions in the tumor volume, which can be assessed by anatomic imaging modalities like CT or MRI. MRI is also capable of detecting changes of the tissue composition within tumors. Diffusion-weighted (DW)-MRI sensitively depicts microstructural reorganizations due to cell swelling and shrinkage. An increase of the apparent diffusion coefficient (ADC) reflects cell death-induced loss of membrane integrity and a relative increase of the extracellular space (4, 5).

Gemcitabine (2',2'-difluorodeoxycytidine, dFdC) is a chemotherapeutic agent employed in, for example, lung (6) or pancreatic cancer (7). It exerts an anticancer effect mostly by interfering with the DNA synthesis. Its metabolites can be

¹European Institute for Molecular Imaging (EIMI), Westfälische Wilhelms-Universität (WWU) Münster, Münster, Germany. ²Department of Clinical Radiology, University Hospital of Münster, Münster, Germany. ³Cancer Research UK Cambridge Institute, University of Cambridge, Cambridge, United Kingdom. ⁴Department of Geriatric Medicine, Johanniter Hospital, Bonn, Germany.

Note: Supplementary data for this article are available at Cancer Research Online (<http://cancerres.aacrjournals.org/>).

Current address for A. Held: Department of Orthopedic Surgery, Otto-von-Guericke University, Magdeburg, Germany; and current address for K. Heinzmann: Comprehensive Cancer Imaging Centre, Imperial College London, London, United Kingdom.

Corresponding Author: Andreas H. Jacobs, European Institute for Molecular Imaging (EIMI), Waldeyerstr. 15, 48149, Münster, Germany. Phone: 49-251-83-49300; Fax: 49-251-83-49313; E-mail: ahjacobs@uni-muenster.de

doi: 10.1158/0008-5472.CAN-16-1479

©2016 American Association for Cancer Research.

incorporated into DNA, thereby abrogating effective DNA synthesis. Furthermore, it inhibits thymidylate synthase (TS), the key enzyme of the thymidine *de novo* synthesis pathway (8, 9). This pathway is the alternative pathway to the thymidine salvage pathway, which is the basis for [¹⁸F]FLT uptake in tissues. It has been shown for other TS-inhibiting agents that a counter-mechanistic upregulation of the salvage pathway results in increased uptake of [¹⁸F]FLT (10, 11).

Here, we investigate whether [¹⁸F]FLT-PET and DW-MRI are suitable methods to detect gemcitabine-induced therapy response in experimental lung cancer xenograft models by employing a gemcitabine-sensitive and -insensitive lung cancer model.

Materials and Methods

Cell culture experiments

A549 (DSMZ) and H1975 (LGC standards, both obtained in December 2011) non-small cell lung cancer cells were cultured at 37°C in 5% CO₂ with DMEM or RPMI, respectively, containing 10% FCS, 100 U/mL penicillin, and 100 µg/mL streptomycin. Cell line identity was confirmed by the supplier by short tandem repeat analysis and the cells were used at an early passage. An MTT assay (Sigma, M5655) was performed according to the manufacturer's protocol to determine the cell viability after gemcitabine administration. Cells were incubated for 48 hours with different concentrations of gemcitabine (0.01 µmol/L–10 µmol/L, Gemzar, Eli Lilly, obtained from the pharmacy of the University Hospital Münster, Münster, Germany).

For *in vitro* [¹⁸F]FLT uptake assays 1.5 × 10⁵ cells per well were seeded in 6-well plates 72 hours prior to the experiment. Gemcitabine at 0.5 µmol/L, 1 µmol/L, or 10 µmol/L concentrations was added 4, 24, or 48 hours, respectively, before the medium was exchanged for 1 hour for medium containing 0.142 MBq/mL [¹⁸F]FLT. After three washing steps, cells were detached, and tracer uptake was determined in a 2480 automatic Gamma Counter "Wallac Wizard2 3" (Perkin Elmer). Cell number was assessed in a Z2 counter particle count and size analyzer (Beckman Coulter). To measure competition between [¹⁸F]FLT and gemcitabine *in vitro*, 5 × 10⁵ cells were seeded the day before the experiment. Cells were incubated with the indicated concentrations of the drug for 1 or 4 hours and then incubated with [¹⁸F]FLT either in the presence (+) or absence (–) of gemcitabine. Tracer uptake was determined as described above.

Western blot analysis

Cells were lysed in RIPA and subjected to PAGE. After transfer to a polyvinylidene difluoride (PVDF) membrane, proteins were probed with antibodies targeting TK1 (Abcam, EPR3193, 1:1,000) or actin (MP Biomedicals, clone C4, 69100, 1:1,000). Secondary antibodies were coupled with peroxidase, and signals were visualized with Pierce ECL Plus Western Blotting Substrate (Pierce Biotechnology). Densitometry analysis of bands was performed with ImageJ and plotted relative to actin-loading control. TK1 expression levels were normalized to the expression of NaCl-treated control cells on the same blot.

Animal model

Animal procedures were performed within the multicenter QuIC-ConCePT study in accordance with the German Laws for Animal Protection and were approved by the Animal Care Committee of the local government (North Rhine-Westphalia State

Agency for Nature, Environment and Consumer Protection). During the experiments, general health and body weight of the mice were monitored. Six- to 8-week-old female NMRI nude mice (Janvier Labs) were used for the experiments. Three tumors per mouse were inoculated subcutaneously in the shoulder region by injection of 2 × 10⁶ cells in 50-µL medium. Tumor volumes were calculated from digital caliper measurements (volume = $\pi/6 \times (L \times W^2)$; *L*, longer diameter; *W*, shorter diameter). Mice were treated by intraperitoneal injection of 100 mg/kg gemcitabine in 100-µL 0.9% NaCl at 3-day intervals or 0.9% NaCl as control. Imaging was performed according to the experimental schedule depicted in Supplementary Fig. S1.

PET imaging

[¹⁸F]FLT was produced with a purity of >99% as reported previously (12). Mice were anesthetized with isoflurane inhalation (2% in oxygen), and temperature was maintained at 37°C by using a heating pad. Radiotracer (10 MBq) was injected intravenously and image acquisition was performed for 20 minutes after a 70-minute tracer uptake period using a quadHIDAC small-animal PET scanner (Oxford Positron Systems; ref. 13). A multimodal bed was used to enable coregistration of PET images with anatomic images from CT (Inveon, Siemens Medical Solutions) or T₂-weighted (T_{2w}) MRI.

Images were analyzed with the software Inveon Research Workplace 3.0 (Siemens Medical Solutions). Three-dimensional volumes-of-interest (VOI) were defined on CT or MR images over the entire tumor. Radiotracer uptake was calculated as the maximal percentage injected dose per mL (%ID_{max}/mL). In addition, we also determined %ID_{mean}/mL, standardized uptake value (SUV_{max} SUV_{mean}), and maximal tumor-to-muscle_{mean} and tumor-to-liver_{mean} ratio. Results of the mean tumor uptake were substantially influenced by necrosis within the tumors. We also assessed the 25th percentile, representing the mean of the 25% highest intensity voxels. All additional evaluations are listed in Supplementary Table S1, and were used to demonstrate that findings were independent of the mode of data analysis. To evaluate relative excretion, the radioactivity within the bladder VOI (%ID_{mean}/mL) was multiplied by the volume of the VOI and divided by the total radioactivity within the mouse.

MR imaging

T_{2w} MR images were obtained with a 9.4 T Bruker Biospec (2D rapid acquisition with relaxation enhancement, repetition/echo time (TR/TE) 3,600/40 ms, rare factor 8, field-of-view (FOV) 35 mm, 256 matrix; slice thickness 1 mm) to obtain anatomic information for the definition of VOIs. ADC was determined by DW-MRI (EPI-DTI, TR/TE 1,000/19 ms, 12 segments, effective b-values = 2, 54, 109, 204, 309, 413, 620, 702 s/mm², FOV 35 mm, 128 matrix, NEX 6, respiration-triggered, slice thickness 1 mm, 4 slices in the tumor center). ADC maps were calculated with the software ParaVision 5.1 (monoexponential fit of all b-values). ImageJ (NIH, Bethesda, MD) was employed to manually segment the tumors in ADC maps and determine the ADC_{mean} of up to 4 slices per tumor.

IHC

Tumors were fixed in 4% paraformaldehyde and embedded in paraffin. Transverse 5-µm sections were incubated overnight at 4°C with primary antibodies (Ki67: Abcam, ab 16667, 1:100; TK1: Abcam, EPR3193, 1:200) and for 1 hour at room temperature

with respective biotin or fluorescently labeled secondary antibodies. Staining was evaluated using a Nikon Eclipse 90i fluorescent microscope and the NIS-Elements software package (Nikon). For quantification, five images at 20 \times resolution were acquired in regions with the highest fraction of specifically stained cells to compare the labeling to radiotracer uptake expressed as %ID_{max}/mL. For Ki67 quantification, stained nuclei relative to the total number of DAPI-stained nuclei were determined. For TK1, the staining-positive area was evaluated after color deconvolution with ImageJ.

Thymidine and gemcitabine quantification

Thymidine was analyzed with a modified LC-MS/MS method as described previously (14). Gemcitabine LC-MS/MS was performed according to Bapiro and colleagues (15).

Statistical analysis

Data are displayed as box plots showing median values with 25th and 75th percentiles, with whiskers from minimum to maximum. Means \pm SD are listed in the Supplementary Table S2. The numbers in brackets indicate the number of samples analyzed. SigmaPlot 13.0 was used for statistical analyses. As not all data followed a normal distribution, the Mann-Whitney rank-sum test was applied for comparisons. IC₅₀ values were determined using the standard curve macro. Correlations were calculated with the Pearson method. *P* values <0.05 were considered statistically significant.

Results

Incubation of H1975 or A549 tumor cells with gemcitabine results in cell death and induction of increased [¹⁸F]FLT uptake *in vitro*

We previously determined that H1975 and A549 lung cancer xenografts accumulate [¹⁸F]FLT and therefore should be suitable to monitor treatment efficacy (16). MTT assays revealed similar half maximum inhibitory concentrations of these two cell lines *in vitro* (IC₅₀[H1975] = 0.33 μ mol/L \pm 0.19 μ mol/L, *n* = 6, IC₅₀[A549] = 0.79 μ mol/L \pm 0.26 μ mol/L, *n* = 4, *P* < 0.05). Thus, both cell lines were responsive to gemcitabine therapy. We performed [¹⁸F]FLT uptake assays *in vitro* to assess whether gemcitabine induces changes in tracer uptake under such conditions (Fig. 1A). No differences in [¹⁸F]FLT accumulation were apparent after 4-hour incubation with the drug. After 24 and 48 hours, [¹⁸F]FLT accumulation was significantly increased in H1975 cells. A similar pattern was observed in gemcitabine-treated A549 cells. However, longer exposure times induced a higher rate of cell death in A549 cells (Fig. 1B), which was accompanied by reduced tracer uptake in this experimental setup. Gemcitabine incubation was accompanied by increased TK1 expression as determined by Western blot analysis (Fig. 1C). Thus, a TK1-associated increase in [¹⁸F]FLT uptake was noted in both cell lines within 24 hours, followed by a drug dose-dependent decrease in A549 cells.

In vivo growth of H1975 is affected by gemcitabine therapy, whereas A549 growth is unaltered

We gave four doses of 100 mg/kg gemcitabine to nude mice bearing subcutaneous H1975 or A549 xenografts of a size of about 100 mm³. A549 xenografts grew substantially more slowly. There was no evidence of gemcitabine-induced toxicity. A growth-inhibitory effect was observed from day 5 onwards for H1975

xenografts, whereas growth of A549 was unaffected (Fig. 2). Thus, a gemcitabine-responsive and a nonresponsive model were available to evaluate the ability of [¹⁸F]FLT-PET and DW-MRI to detect any effects of gemcitabine treatment on the tumors.

Gemcitabine affects [¹⁸F]FLT uptake in both models *in vivo*

We performed [¹⁸F]FLT-PET imaging at various time points after administration of gemcitabine (Fig. 3). In both tumor types, tracer uptake was significantly reduced within hours after drug application and significantly increased on day 1 (%ID_{max}/mL of H1975: baseline: 18.6 \pm 3.3, 6 hours: 9.8 \pm 2.0, *P* < 0.001; day 1: 21.5 \pm 3.2, *P* < 0.01; A549: baseline: 6.39 \pm 1.57, 6 hours: 3.68 \pm 0.68, *P* < 0.001; day 1: 8.95 \pm 2.75, *P* < 0.001, significances relative to baseline; see Supplementary Table S2 for all numbers). On day 2 and 3, [¹⁸F]FLT uptake was equal to baseline and to respective NaCl controls. A significant reduction in [¹⁸F]FLT uptake could be noted in H1975 xenografts on day 5 of gemcitabine therapy (15.0 \pm 3.4, *P* < 0.01 relative to baseline). In contrast to all other observations, the slight increase of [¹⁸F]FLT uptake in H1975 tumors on day 2 and in A549 xenografts on day 5 could not be confirmed with most other [¹⁸F]FLT uptake parameters (see Supplementary Table S1).

We analyzed Ki67 IHC to assess whether [¹⁸F]FLT accumulation reflects cellular proliferation. In both tumor models, Ki67 was unchanged after gemcitabine therapy (Fig. 4; Supplementary Fig. S2). Unaltered [¹⁸F]FLT on day 2 and 3 was in accordance with unchanged cellular proliferation as determined by Ki67 IHC. The cause for the above described changes in [¹⁸F]FLT uptake (i.e., decrease after 6 hours, increase after 1 day, and decrease after 5 days in H1975 xenografts) appeared to be unrelated to this proliferation marker.

Immunohistochemical analysis revealed an increased TK1 expression on day 1 after gemcitabine (%positive area of H1975: NaCl: 21.5 \pm 5.0, day 1: 45.1 \pm 8.8; A549: NaCl: 19.9 \pm 5.8, day 1: 36.8 \pm 4.3; both *P* < 0.01 relative to NaCl control). A significant positive correlation of TK1 expression and [¹⁸F]FLT uptake was measured in both models (Fig. 5). Of note, for the H1975 tumors, PET imaging after 6 hours was only performed in longitudinal studies. Hence, IHC at this time point was conducted in a different cohort of mice, not allowing direct correlation analysis of this time point. For consistency, we did not plot this time point for A549 either; however, inclusion of these 6-hour data also results in a significant correlation of [¹⁸F]FLT uptake and TK1 expression (*r* = 0.539, *P* < 0.01).

[¹⁸F]FLT uptake after 6 hours in tumors was low although TK1 expression was elevated. Also TS or human equilibrative nucleoside transporter 1 (hENT1) expression analysis did not explain reduced [¹⁸F]FLT (Supplementary Fig. S3). Interestingly, not only tumor uptake was reduced at this time point but [¹⁸F]FLT retention in a range of other organs was also diminished (e.g., spleen, muscle, or lymph nodes, see Supplementary Table S3), indicating a potential systemic rather than a tumor-specific effect. Gemcitabine, being a nucleoside analogue, employs cellular transport mechanisms similar to the ones used by [¹⁸F]FLT and thymidine. Hence, we hypothesized that high gemcitabine concentrations in the plasma compete with [¹⁸F]FLT for cellular uptake.

We showed that less [¹⁸F]FLT is taken up by cells in the presence of gemcitabine *in vitro* (Fig. 6A), confirming the competitive nature of these two molecules. *In vivo*, LC-MS/MS analysis revealed gemcitabine (dFdC) tumor concentrations of 3.38

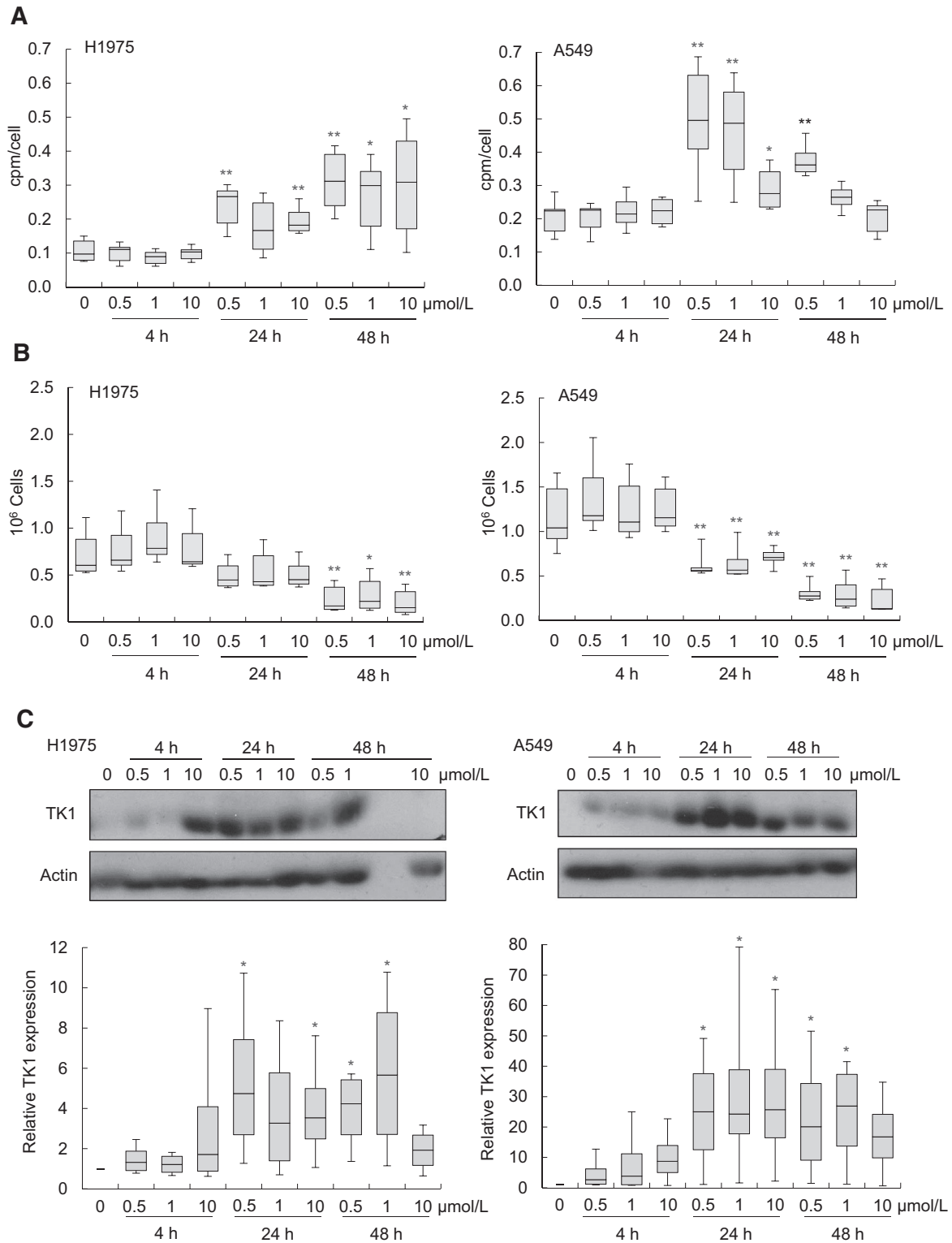


Figure 1. Gemcitabine induced an increase in uptake of [¹⁸F]FLT in H1975 and A549 tumor cells *in vitro*. **A**, [¹⁸F]FLT uptake assays revealed elevated radiotracer retention after prolonged treatment with gemcitabine in both cell lines. Tracer accumulation is expressed as counts per minute (cpm) per cell. **B**, Cell number is displayed as an indicator of cell viability after gemcitabine therapy. Boxplots depict medians of six values obtained in three individual experiments. **C**, Western blot analysis of cell lysates revealed increased expression of TK1 after gemcitabine treatment. *n* = 4 samples were analyzed per condition (*, *P* < 0.05; **, *P* < 0.01 relative to NaCl control).

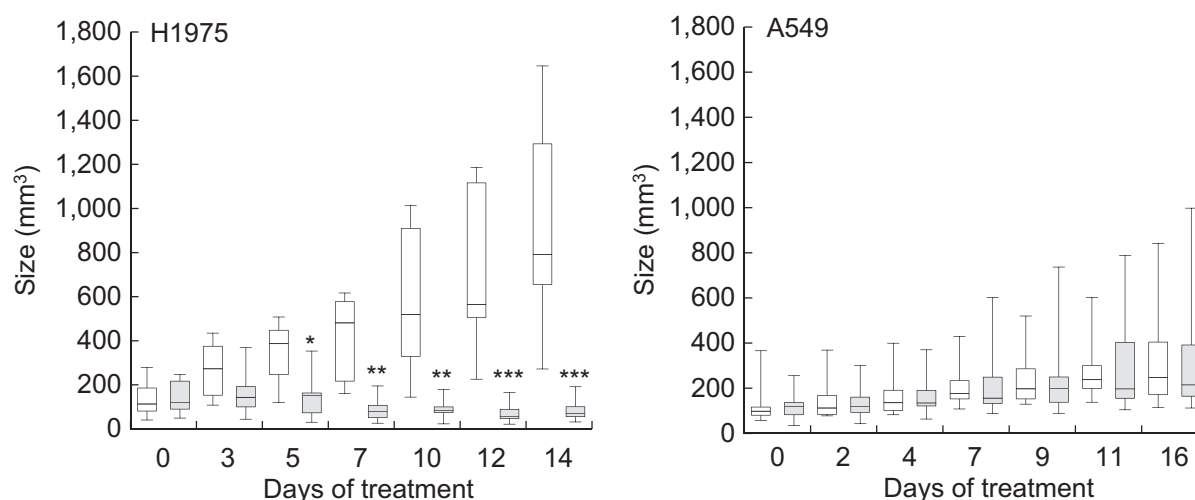


Figure 2.

Gemcitabine therapy induced growth inhibition in H1975 but not in A549 xenografts. Tumor volumes were determined by caliper measurements and showed a growth-inhibitory effect of gemcitabine (given on day 0, 3, 6, and 9) in H1975 but not in A549 tumors. White, NaCl; gray, gemcitabine (*, $P < 0.05$; **, $P < 0.01$; ***, $P < 0.001$ relative to NaCl).

$\mu\text{mol/L} \pm 2.34 \mu\text{mol/L}$ in H1975 ($n = 4$) and approximately $1.2 \mu\text{mol/L}$ in A549 ($n = 2$) and plasma concentrations in the range of $0.16 \mu\text{mol/L} \pm 0.08 \mu\text{mol/L}$ ($n = 5$) 6 hours after drug administration. The latter is well above the concentrations estimated for [^{18}F]FLT ($\sim 0.01 \mu\text{mol/L}$) and could effectively reduce the amount of [^{18}F]FLT taken up by cells. Consequently, as less [^{18}F]FLT was taken up and retained in cells throughout the body, more tracer should be excreted. By quantifying the amount of tracer within the bladder, we showed that more [^{18}F]FLT was excreted 6 hours after gemcitabine administration (% [^{18}F]FLT in bladder: baseline: 13.7 ± 5.8 , 6 hours: 24.8 ± 6.5 , $P < 0.05$, Fig. 6B). Thymidine also employs the cellular uptake mechanism for nucleosides. Plasma concentration of thymidine was significantly higher at 6 hours (Fig. 6C). On the basis of its short half-life (~ 30 minutes; refs. 17, 18), plasma gemcitabine concentrations should be in the range of approximately $500 \mu\text{mol/L}$ immediately after drug administration. This approximately 500-fold excess of gemcitabine over plasma thymidine suggests that increased thymidine concentrations after 6 hours result from competition with gemcitabine. At later time points, plasma thymidine levels were significantly reduced relative to NaCl control, whereas thymidine concentrations within H1975 tumors were increased (Fig. 6D).

ADC is slightly altered early after gemcitabine administration

We also determined whether gemcitabine application causes changes in the apparent diffusion coefficient (ADC), the measure for water diffusivity as determined by DW-MRI. Figure 7A shows that ADC_{mean} did not vary substantially on day 1 or 2 after treatment in H1975 xenografts. In A549 tumors, a small increase in ADC relative to the baseline was detected, which was independent of the treatment. This increase was more pronounced 1 day after gemcitabine administration. However, in both models, cellular density (Fig. 7B) and cell death (cleaved caspase-3 IHC, Supplementary Fig. S4) were not altered at these time points.

Discussion

We employed two lung cancer models to investigate the effect of gemcitabine on [^{18}F]FLT-PET and DW-MRI. The two models differed with respect to gemcitabine sensitivity *in vivo*. We observed a growth inhibition–related decrease of [^{18}F]FLT uptake on day 5 of treatment in the sensitive H1975 xenografts. Early changes in tracer uptake (within hours and on day 1), as well as ADC, were not related to treatment response. These results indicate that a detailed understanding of the various mechanisms determining changes in imaging biomarkers is important when interpreting such changes for the analysis of therapy response, especially at early time points. With regards to gemcitabine, the mechanisms influencing [^{18}F]FLT uptake are rather complex, as elucidated here.

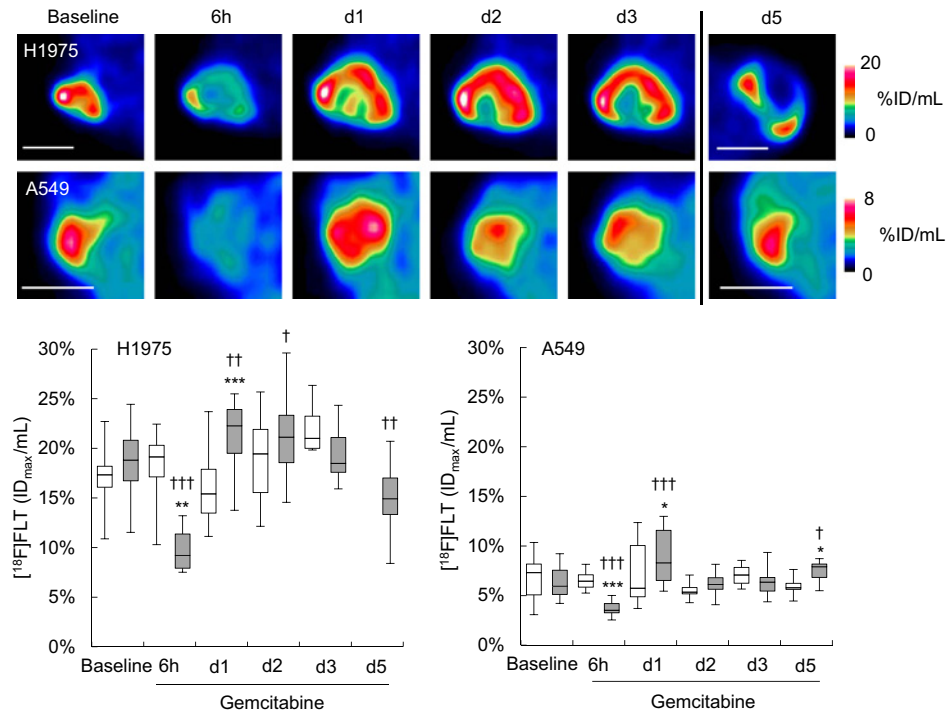
There is a range of studies describing the successful use of [^{18}F]FLT-PET for predicting response to anticancer agents (19, 20). When employing agents interfering with TS activity, like 5-fluorouracil (5-FU), an increase in [^{18}F]FLT uptake early after drug administration was frequently reported. This effect has been attributed either to upregulation of TK1 activity (10, 11) or to redistribution of hENT1 to the cellular surface (21).

Gemcitabine also inhibits TS activity (8). Consequentially, we also observed an [^{18}F]FLT increase both *in vitro* (Fig. 1) and *in vivo* (Fig. 3). This is in accordance with an *in vitro* study that reported a 5-fold increase of [^{18}F]FLT 24 hours after treatment with gemcitabine in esophageal squamous cell carcinoma cells (22). In our models, we showed that increased [^{18}F]FLT was related to TK1 expression (Figs. 1C and 5).

We noted a substantial decrease of tumor [^{18}F]FLT accumulation 6 hours after gemcitabine administration (Fig. 3). This reduction was not related to the expression of Ki67, TK1, TS, or hENT1. Our *in vivo* data indicate that competition of gemcitabine uptake with [^{18}F]FLT is most likely the cause for the reduced [^{18}F]FLT uptake, as also demonstrated by *in vitro* [^{18}F]FLT uptake experiments (Fig. 6A). Both molecules share cellular uptake mechanisms, and the major transporter is presumably hENT1. Expression of hENT1 predicts gemcitabine response in patients

Figure 3.

PET showed reduced uptake of [¹⁸F]FLT 6 hours after gemcitabine administration and increased uptake after 1 day, whereas a growth inhibition-related reduction in H1975 tumors could only be noted on day 5. Static [¹⁸F]FLT-PET was performed at the indicated time points after gemcitabine treatment. Notably, for the 6-hour time point, the tracer was injected about 4 hours after drug administration. The PET image was acquired 70–90 minutes after tracer injection during the sixth hour after drug application. Images show transverse slices at the biggest tumor diameter of one representative H1975 or A549 tumor over time. This longitudinal study did not include the day 5 time point. Hence, the images from day 5 depict different tumors. Scale bar, 5 mm; white, NaCl; gray, gemcitabine (*, *P* < 0.05; **, *P* < 0.01; ***, *P* < 0.001 relative to NaCl; †, *P* < 0.05; ††, *P* < 0.01; †††, *P* < 0.001 relative to baseline).



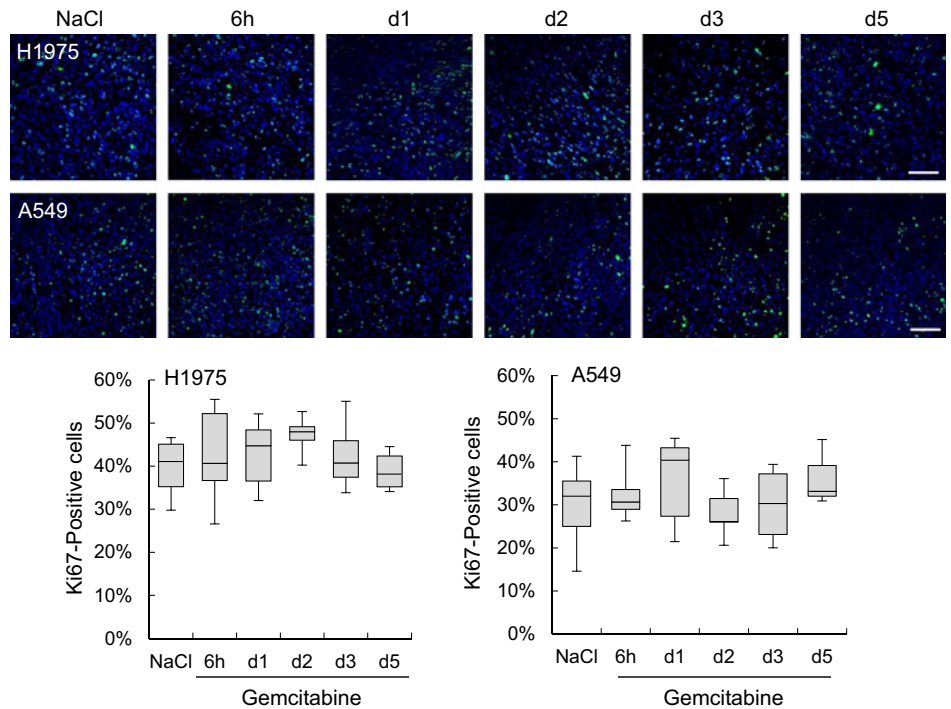
with biliary tract cancer (23), cholangiocarcinoma (24), or pancreatic cancer (25). Furthermore, Paproski and colleagues demonstrated that [³H]FLT uptake predicts transport and toxicity of gemcitabine in a range of pancreatic cancer cell lines *in vitro* (26). We determined gemcitabine plasma concentrations to be approximately 160 nmol/L about 6 hours after drug application. This is in good agreement with the previously published gemcitabine concentrations (15, 27). According to Zhang and colleagues,

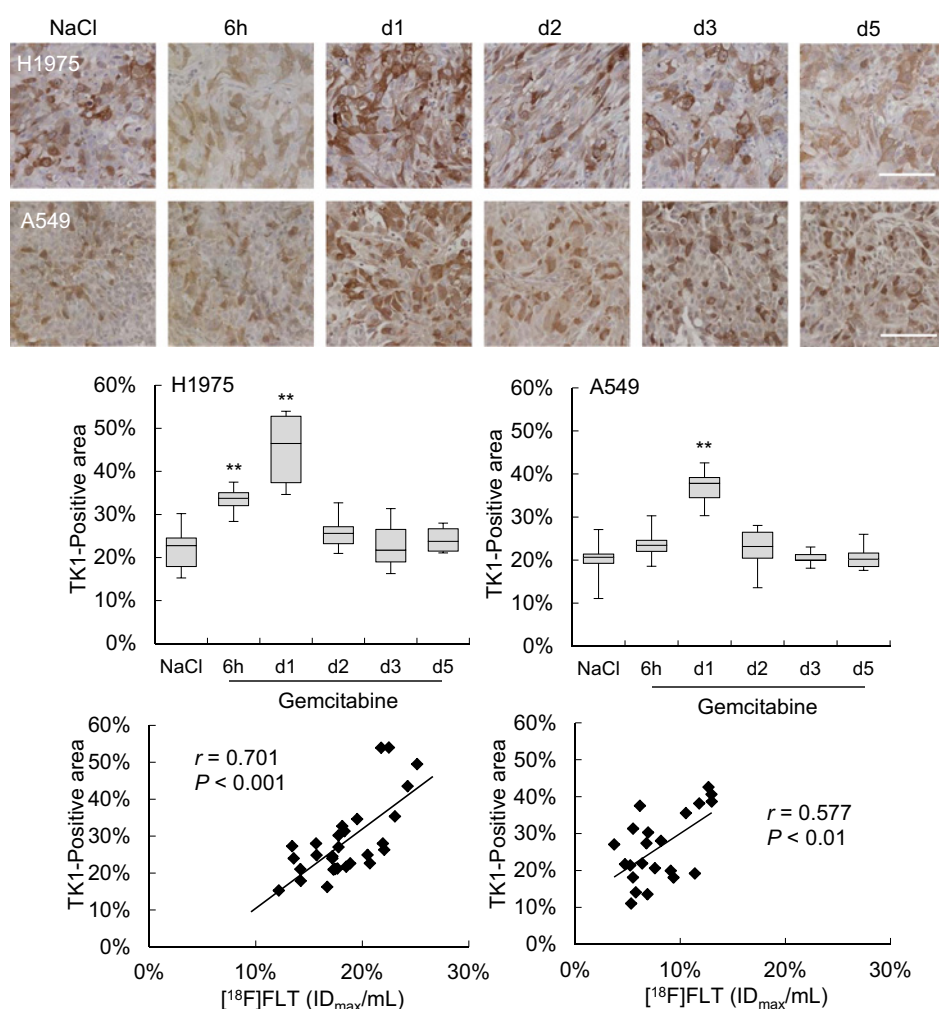
the estimated dose level of [¹⁸F]FLT used in preclinical imaging is 2 μg/kg (8.2 nmol/L) (28), resulting in competition of [¹⁸F]FLT and gemcitabine for cellular transport mechanisms, which could be measured by PET and gamma counter measurements in our study.

We showed that less [¹⁸F]FLT accumulated in a range of organs 6 hours after gemcitabine administration because less tracer was taken up by the cells. Hence, more [¹⁸F]FLT would be excreted and

Figure 4.

Ki67 is unaltered after gemcitabine treatment. H1975 and A549 tumor sections were stained for Ki67 as described in Materials and Methods. Scale bar, 100 μm. Green, Ki67; blue, DAPI.



**Figure 5.**

TK1 expression was correlated with [^{18}F]FLT uptake. IHC analysis revealed a significant upregulation of TK1 one day after administration of a single dose of gemcitabine in H1975 and A549 xenografts. Sections were stained in different batches, explaining the variations in color. Scale bar, 100 μm . There is a significant positive correlation of TK1 staining and [^{18}F]FLT uptake in both xenograft models (6-hour values were omitted for correlation analysis; **, $P < 0.01$ relative to NaCl).

indeed the amount of [^{18}F]FLT in the bladder increased by about 70% (Fig. 6B). One might speculate that such a systemic effect on tracer uptake calls for correction of [^{18}F]FLT uptake to an internal reference tissue. But after also correcting for muscle or liver uptake, the relative decrease in tumor [^{18}F]FLT accumulation remained significant (Supplementary Table S1). This implies that gemcitabine is preferentially taken up in tumors, in agreement with a study demonstrating a 3.5-fold increased accumulation of gemcitabine relative to liver (18). Hence, there are multiple pieces of evidence that support the hypothesis that 6 hours after administration, gemcitabine competes with [^{18}F]FLT for cellular uptake.

We also observed competition of gemcitabine with plasma thymidine 6 hours after drug administration (Fig. 6C). Day 1, 2, and 3 after gemcitabine, plasma thymidine concentrations were reduced relative to the NaCl control. This is in line with other studies employing TS-inhibiting agents that showed reduced thymidine levels in plasma in mice (29) and men (30), presumably originating from the drug-induced blockade of the *de novo* pathway and increased use of the salvage pathway and hence extracellular thymidine. A significant increase in thymidine concentration was noted in H1975 xenografts. This could possibly be caused by an accumulation of phosphorylated thymidine within the cells, which cannot be incorporated into the DNA as gemcitabine inhibits DNA synthesis. The fact that this increase in

thymidine cannot be detected in A549 xenografts, whose growth is not impaired after gemcitabine treatment, supports this hypothesis.

Of note, changes in [^{18}F]FLT uptake and TK1 expression within the first days were observed in both tumor models investigated, even though they substantially differed with respect to sensitivity to gemcitabine (Fig. 2). Gemcitabine concentrations within A549 tumors were in a similar range to those in H1975 tumors, demonstrating that gemcitabine is capable of entering these cells. A double dose of gemcitabine did cause a reduction in tumor volume in a small cohort of mice (Supplementary Fig. S5). Hence, as previously reported (31, 32), A549 xenografts were not intrinsically resistant to this drug, but in our study, the dose used was subtherapeutic. Consequently, the observed early changes in [^{18}F]FLT uptake (reduction after 6 hours and increase after 1 day) were not related to treatment response. This is in accordance with studies showing that subtherapeutic doses of TS-inhibiting agents induce an [^{18}F]FLT increase *in vitro* (33) and *in vivo* (34).

A growth inhibition-related decrease in [^{18}F]FLT uptake was only seen on day 5 of gemcitabine therapy. Presumably, this was related to increased apoptosis as determined by IHC of cleaved caspase-3 (Supplementary Fig. S4). In our study, H1975 tumor volumes between the treated and the untreated groups were already significantly different on day 5. Hence, molecular imaging

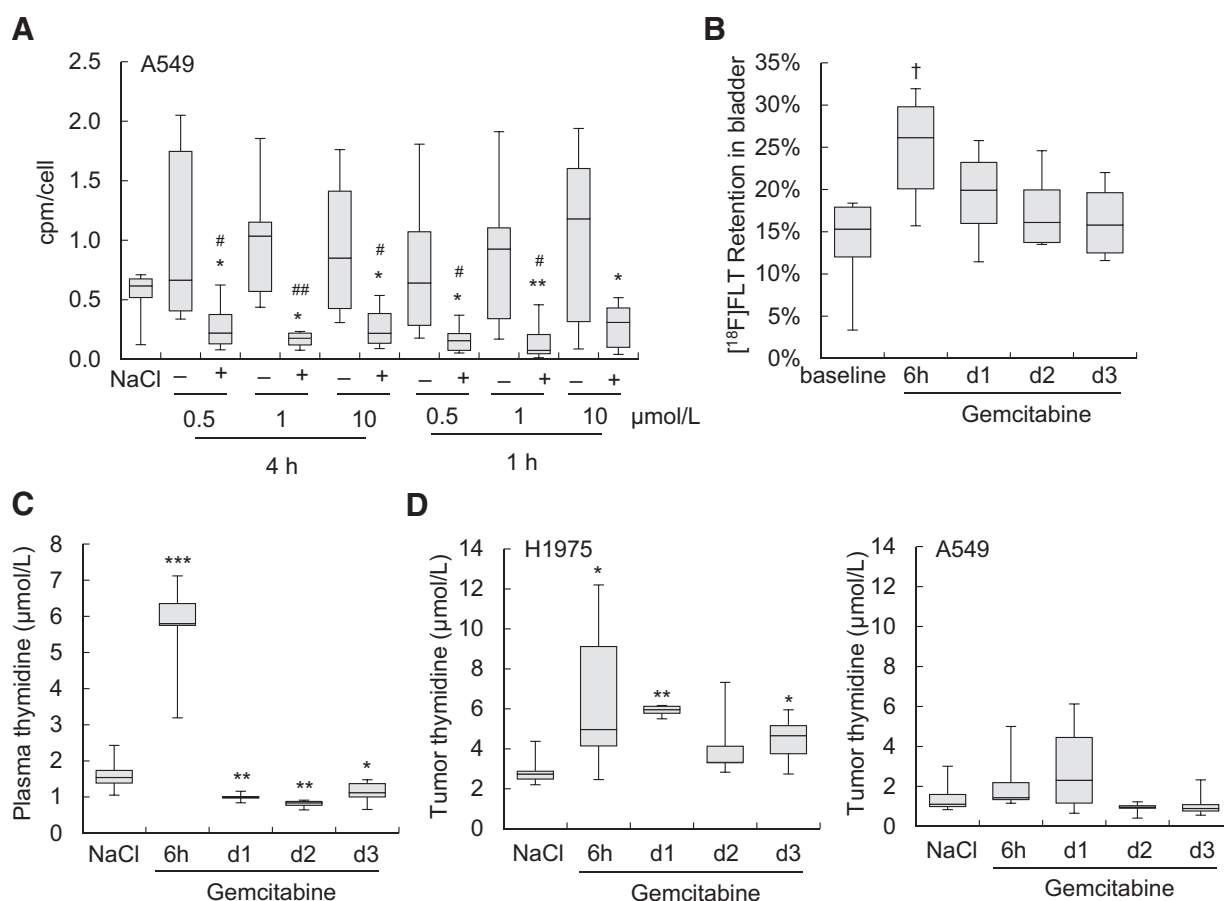


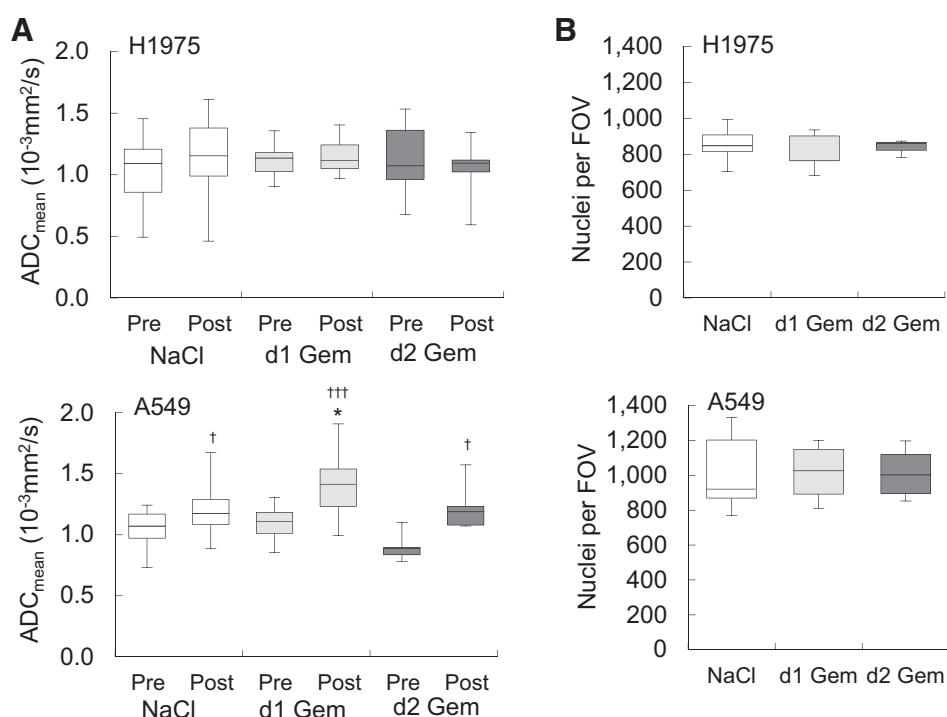
Figure 6. Gemcitabine competed with [¹⁸F]FLT *in vitro* and increased [¹⁸F]FLT excretion and plasma thymidine levels after 6 hours *in vivo*. **A**, A549 cells were incubated with different concentrations of gemcitabine for 1 or 4 hours. Subsequently, [¹⁸F]FLT uptake was determined either in the presence (+) or absence (–) of gemcitabine. Median values of *n* = 6 values, obtained in three different experiments, are displayed here. **B**, Excretion of [¹⁸F]FLT was assessed by calculating the tracer amount within the bladder relative to the radioactivity within the mouse. Data from mice bearing different tumor types were pooled. **C** and **D**, Plasma (**C**) and tumor thymidine (**D**) were quantified with an LC-MS/MS method. The plasma results from mice bearing different tumor types were pooled because the tumor appeared not to affect plasma thymidine concentration (*, *P* < 0.05; **, *P* < 0.01; ***, *P* < 0.001 relative to NaCl; †, *P* < 0.05 relative to baseline); #, *P* < 0.05; ##, *P* < 0.01 relative to respective uptake in absence of gemcitabine.

with [¹⁸F]FLT-PET would not provide additional (earlier) information over volume measurements. However, findings on timing from preclinical studies cannot be directly transferred to the clinical situation. In general, clinical tumors grow more slowly than preclinical xenografts. This could result in reductions in [¹⁸F]FLT occurring prior to reductions in tumor volume. Consequently, [¹⁸F]FLT-PET could potentially be used for the assessment of treatment response in cancer patients treated with gemcitabine, if imaging is not performed within the first days of therapy. Moreover, a detailed kinetic analysis deciphering [¹⁸F]FLT delivery and transport (*K*₁) from the rate of phosphorylation (*k*₃) could be envisioned to especially shed light into gemcitabine action on [¹⁸F]FLT metabolism in clinical applications.

In our study, results were obtained from mice bearing several tumors. The advantage of this model system is that according to the principles of the 3Rs (replacement, reduction, refinement) the number of animals can be reduced. Most importantly, the tracer input function is the same for tumors growing in the

same animal. Therefore, differences in [¹⁸F]FLT uptake can be attributed to differences in tumor growth (location, vascularization, biologic activity) and not to potential differences in the imaging protocol. However, one has to bear in mind, that analyses of mice bearing single xenografts could potentially better reflect the clinical situation with its interindividual biological heterogeneities.

DW-MRI is an alternative imaging approach to monitor cancer therapy, as has been shown, for example, for experimental Ewing sarcoma (35). We were unable to detect any substantial differences in tumor ADC_{mean} 1 or 2 days after a single dose of gemcitabine in either of the lung tumor models investigated here (Fig. 7A). This was in accordance with unchanged cellular density and cell death. The slight increase in ADC in A549 xenografts most likely resulted from other structural changes such as a growth-related increase in necrosis, which was irrespective of treatment. These observations emphasize that ADC is a versatile measure that is influenced by a complex combination of parameters related to tissue microstructure. Transient effects such as cell swelling or

**Figure 7.**

ADC was not altered after gemcitabine therapy in H1975, which was in line with unchanged cellular density. **A**, The ADC_{mean} of up to four transverse tumor sections was determined and averaged. **B**, Cellular density was determined by counting DAPI-positive nuclei in 20× fields of view (FOV, 580 μm × 460 μm) on Ki67 histology sections. White, NaCl; light gray, one day after gemcitabine; dark gray, two days after gemcitabine; Gem, gemcitabine; *, *P* < 0.05 relative to NaCl; †, *P* < 0.05; ††, *P* < 0.005 relative to baseline.

shrinkage possibly overshadow changes of parameters that can be related to therapy with our current knowledge. Hence, in our model, ADC had no predictive value.

In conclusion, our data demonstrate that plasma levels of gemcitabine alter nucleoside transporter availability and hence [¹⁸F]FLT uptake early after gemcitabine administration. Moreover, molecular factors like TK1 activity might hamper the straightforward noninvasive detection of early treatment effects by [¹⁸F]FLT-PET when employing agents inhibiting TS. Hence, understanding the mechanism of action of a therapeutic approach as well as the mechanisms of [¹⁸F]FLT uptake are crucial for interpreting respective PET imaging findings.

Disclosure of Potential Conflicts of Interest

No potential conflicts of interest were disclosed.

Authors' Contributions

Conception and design: S. Schelhaas, J.R. Griffiths, A.H. Jacobs

Acquisition of data (provided animals, acquired and managed patients, provided facilities, etc.): S. Schelhaas, A. Held, L. Wachsmuth, D.J. Honess, D.-M. Smith, C. Faber

Analysis and interpretation of data (e.g., statistical analysis, biostatistics, computational analysis): S. Schelhaas, A. Held, L. Wachsmuth, S. Hermann, D.J. Honess, K. Heinzmann, C. Faber

Writing, review, and/or revision of the manuscript: S. Schelhaas, L. Wachsmuth, S. Hermann, D.J. Honess, K. Heinzmann, D.-M. Smith, J.R. Griffiths, C. Faber, A.H. Jacobs

Study supervision: S. Schelhaas, A.H. Jacobs

Acknowledgments

We acknowledge Christine Bätza, Stefanie Bouma, Florian Breuer, Irmgard Hoppe, Sarah Köster, Nina Kreienkamp, Christa Möllmann, Roman Priebe, and Dirk Reinhardt for excellent technical assistance and the Interdisciplinary Centre for Clinical Research (IZKF, core unit PIX), Münster, Germany.

Grant Support

The research leading to these results has received support from the Innovative Medicines Initiative Joint Undertaking (www.imi.europa.eu) under grant agreement number 115151, resources of which are composed of financial contribution from the European Union's Seventh Framework Programme (FP7/2007-2013) and EFPIA companies' in kind contribution. This work was also supported by the Deutsche Forschungsgemeinschaft (DFG), Cells-in-Motion Cluster of Excellence (EXC1003 - CiM), University of Münster (Münster, Germany).

The costs of publication of this article were defrayed in part by the payment of page charges. This article must therefore be hereby marked *advertisement* in accordance with 18 U.S.C. Section 1734 solely to indicate this fact.

Received May 24, 2016; revised October 13, 2016; accepted October 17, 2016; published OnlineFirst October 26, 2016.

References

1. Been LB, Suurmeijer AJH, Cobben DCP, Jager PL, Hoekstra HJ, Elsinga PH. [¹⁸F]FLT-PET in oncology: current status and opportunities. *Eur J Nucl Med Mol Imaging* 2004;31:1659-72.
2. Chalkidou A, Landau DB, Odell EW, Cornelius VR, O'Doherty MJ, Marsden PK. Correlation between Ki-67 immunohistochemistry and [¹⁸F]fluorothymidine uptake in patients with cancer: a systematic review and meta-analysis. *Eur J Cancer* 2012;48:3499-513.
3. Soloviev D, Lewis D, Honess D, Aboagye E. [(18)F]FLT: an imaging biomarker of tumour proliferation for assessment of tumour response to treatment. *Eur J Cancer* 2012;48:416-24.
4. Sinkus R, Van Beers BE, Vilgrain V, DeSouza N, Waterton JC. Apparent diffusion coefficient from magnetic resonance imaging as a biomarker in oncology drug development. *Eur J Cancer* 2012;48:425-31.

5. Le Bihan D, Lima M. Diffusion magnetic resonance imaging: what water tells us about biological tissues. *PLoS Biol* 2015;13:e1002203.
6. Reynolds JK, Levien TL. Quality-of-life assessment in phase III clinical trials of gemcitabine in non-small-cell lung cancer. *Drugs Aging* 2008;25:893–911.
7. de Sousa Cavalcante L, Monteiro G. Gemcitabine: metabolism and molecular mechanisms of action, sensitivity and chemoresistance in pancreatic cancer. *Eur J Pharmacol* 2014;741:8–16.
8. Honeywell RJ, Ruiz van Haperen VWT, Veerman G, Smid K, Peters GJ. Inhibition of thymidylate synthase by 2',2'-difluoro-2'-deoxycytidine (Gemcitabine) and its metabolite 2',2'-difluoro-2'-deoxyuridine. *Int J Biochem Cell Biol* 2015;60:73–81.
9. Mini E, Nobili S, Caciagli B, Landini I, Mazzei T. Cellular pharmacology of gemcitabine. *Ann Oncol* 2006;17:v7–12.
10. Lee SJ, Kim SY, Chung JH, Oh SJ, Ryu JS, Hong YS, et al. Induction of thymidine kinase 1 after 5-fluorouracil as a mechanism for 3'-deoxy-3'-[¹⁸F]fluorothymidine flare. *Biochem Pharmacol* 2010;80:1528–36.
11. Hong IK, Kim SY, Chung JH, Lee SJ, Oh SJ, Lee SJ, et al. 3'-Deoxy-3'-[¹⁸F]fluorothymidine positron emission tomography imaging of thymidine kinase 1 activity after 5-fluorouracil treatment in a mouse tumor model. *Anticancer Res* 2014;34:759–66.
12. Viel T, Schelhaas S, Wagner S, Wachsmuth L, Schwegmann K, Kuhlmann M, et al. Early assessment of the efficacy of temozolomide chemotherapy in experimental glioblastoma using [¹⁸F]FLT-PET imaging. *PLoS One* 2013;8:e67911.
13. Schäfers KP, Reader AJ, Kriens M, Knoess C, Schober O, Schäfers M. Performance evaluation of the 32-module quadHIDAC small-animal PET scanner. *J Nucl Med* 2005;46:996–1004.
14. Heinzmann K, Honess DJ, Lewis DY, Smith D-M, Cawthorne C, Keen H, et al. The relationship between endogenous thymidine concentrations and [(18)F]FLT uptake in a range of preclinical tumour models. *EJNMMI Res* 2016;6:63.
15. Bapiro TE, Richards FM, Goldgraben MA, Olive KP, Madhu B, Frese KK, et al. A novel method for quantification of gemcitabine and its metabolites 2',2'-difluorodeoxyuridine and gemcitabine triphosphate in tumour tissue by LC-MS/MS: comparison with (19)F NMR spectroscopy. *Cancer Chemother Pharmacol* 2011;68:1243–53.
16. Schelhaas S, Wachsmuth L, Viel T, Honess DJ, Heinzmann K, Smith D-M, et al. Variability of proliferation and diffusion in different lung cancer models as measured by 3'-deoxy-3'-18F-fluorothymidine PET and diffusion-weighted MR imaging. *J Nucl Med* 2014;55:983–8.
17. Veerman G, Ruiz van Haperen VW, Vermorken JB, Noordhuis P, Braakhuis BJ, Pinedo HM, et al. Antitumor activity of prolonged as compared with bolus administration of 2',2'-difluorodeoxycytidine *in vivo* against murine colon tumors. *Cancer Chemother Pharmacol* 1996;38:335–42.
18. Wang H, Li M, Rinehart JJ, Zhang R. Pretreatment with dexamethasone increases antitumor activity of carboplatin and gemcitabine in mice bearing human cancer xenografts: *in vivo* activity, pharmacokinetics, and clinical implications for cancer chemotherapy. *Clin Cancer Res* 2004;10:1633–44.
19. Jensen MM, Kjaer A. Monitoring of anti-cancer treatment with (18)F-FDG and (18)F-FLT PET: a comprehensive review of pre-clinical studies. *Am J Nucl Med Mol Imaging* 2015;5:431–56.
20. Schelhaas S, Heinzmann K, Bollineni VR, Kramer GM, Liu Y, Waterton JC, et al. Preclinical applications of 3'-deoxy-3'-[¹⁸F]fluorothymidine in oncology - a systematic review. *Theranostics* 2017;7:40–50.
21. Perumal M, Pillai RG, Barthel H, Leyton J, Latigo JR, Forster M, et al. Redistribution of nucleoside transporters to the cell membrane provides a novel approach for imaging thymidylate synthase inhibition by positron emission tomography. *Cancer Res* 2006;66:8558–64.
22. Dittmann H, Dohmen BM, Kehlbach R, Bartusek G, Pritzkow M, Sarbia M, et al. Early changes in [¹⁸F]FLT uptake after chemotherapy: an experimental study. *Eur J Nucl Med Mol Imaging* 2002;29:1462–9.
23. Santini D, Schiavon G, Vincenzi B, Cass CE, Vasile E, Manazza AD, et al. Human equilibrative nucleoside transporter 1 (hENT1) levels predict response to gemcitabine in patients with biliary tract cancer (BTC). *Curr Cancer Drug Targets* 2011;11:123–9.
24. Borbath I, Verbrugge L, Lai R, Gigot JF, Humblet Y, Piessevaux H, et al. Human equilibrative nucleoside transporter 1 (hENT1) expression is a potential predictive tool for response to gemcitabine in patients with advanced cholangiocarcinoma. *Eur J Cancer* 2012;48:990–6.
25. Greenhalf W, Ghaneh P, Neoptolemos JP, Palmer DH, Cox TF, Lamb RF, et al. Pancreatic cancer hENT1 expression and survival from gemcitabine in patients from the ESPAC-3 trial. *J Natl Cancer Inst* 2014;106:djt347.
26. Paproski RJ, Young JD, Cass CE. Predicting gemcitabine transport and toxicity in human pancreatic cancer cell lines with the positron emission tomography tracer 3'-deoxy-3'-fluorothymidine. *Biochem Pharmacol* 2010;79:587–95.
27. Awasthi N, Zhang C, Schwarz AM, Hinz S, Wang C, Williams NS, et al. Comparative benefits of Nab-paclitaxel over gemcitabine or polysorbate-based docetaxel in experimental pancreatic cancer. *Carcinogenesis* 2013;34:2361–9.
28. Zhang CC, Yan Z, Li W, Kuszpit K, Painter CL, Zhang Q, et al. [(18)F]FLT-PET imaging does not always "light up" proliferating tumor cells. *Clin Cancer Res* 2012;18:1303–12.
29. Clarke SJ, Farrugia DC, Aherne GW, Pritchard DM, Benstead J, Jackman AL. Balb/c mice as a preclinical model for raltitrexed-induced gastrointestinal toxicity. *Clin Cancer Res* 2000;6:285–96.
30. Li KM, Rivory LP, Hoskins J, Sharma R, Clarke SJ. Altered deoxyuridine and thymidine in plasma following capecitabine treatment in colorectal cancer patients. *Br J Clin Pharmacol* 2007;63:67–74.
31. Kim I-Y, Kang Y-S, Lee DS, Park H-J, Choi E-K, Oh Y-K, et al. Antitumor activity of EGFR targeted pH-sensitive immunoliposomes encapsulating gemcitabine in A549 xenograft nude mice. *J Control Release* 2009;140:55–60.
32. Zundelevich A, Elad-Sfadia G, Haklai R, Kloog Y. Suppression of lung cancer tumor growth in a nude mouse model by the Ras inhibitor salirasib (farnesylthiosalicylic acid). *Mol Cancer Ther* 2007;6:1765–73.
33. Yau K, Price P, Pillai RG, Aboagye E. Elevation of radiolabelled thymidine uptake in RIF-1 fibrosarcoma and HT29 colon adenocarcinoma cells after treatment with thymidylate synthase inhibitors. *Eur J Nucl Med Mol Imaging* 2006;33:981–7.
34. Viertl D, Bischof Delaloye A, Lanz B, Poitry-Yamate C, Gruetter R, Mlynarik V, et al. Increase of [(18)F]FLT tumor uptake *in vivo* mediated by FdUrd: toward improving cell proliferation positron emission tomography. *Mol Imaging Biol* 2011;13:321–31.
35. Reichardt W, Juettner E, Uhl M, Elverfeldt DV, Kontny U. Diffusion-weighted imaging as predictor of therapy response in an animal model of Ewing sarcoma. *Invest Radiol* 2009;44:298–303.